Physics and Astronomy Faculty Publications

Physics and Astronomy

2-1-2007

The Structure of the Homunculus. II. Modeling the Physical Conditions in η Carinae's Molecular Shell

Nathan Smith
University of Colorado

Gary J. Ferland
University of Kentucky, gary@uky.edu

Right click to open a feedback form in a new tab to let us know how this document benefits you.

Follow this and additional works at: https://uknowledge.uky.edu/physastron_facpub

Part of the Astrophysics and Astronomy Commons, and the Physics Commons

The Structure of the Homunculus. II. Modeling the Physical Conditions in η Carinae's Molecular Shell

THE STRUCTURE OF THE HOMUNCULUS. II. MODELING THE PHYSICAL CONDITIONS IN η CARINAE'S MOLECULAR SHELL[1]

Nathan Smith[2,3]

Center for Astrophysics and Space Astronomy, University of Colorado, Boulder, CO

and

Gary J. Ferland

Department of Physics and Astronomy, University of Kentucky, Lexington, KY; gary@pa.uky.edu

Received 2006 July 25; accepted 2006 October 16

ABSTRACT

We present models that reproduce the observed double-shell structure of the Homunculus Nebula around η Carinae, including the stratification of infrared H_2 and [Fe II] emission seen in data obtained with the Phoenix spectrograph on Gemini South, as well as the corresponding stratified grain temperature seen in thermal-infrared data. Tuning the model to match the observed shell thickness allows us to determine the threshold density that permits survival of H_2. An average density of $n_H \simeq (0.5–1) \times 10^7$ cm^{-3} in the outer zone is required to allow H_2 to exist at all latitudes in the nebula, and for Fe$^+$ to recombine to Fe^0. This gives independent confirmation of the very large mass of the Homunculus, indicating a total of roughly 15–35 $M_\odot$ (although we note reasons why the lower end of this range is favored). At the interface between the atomic and molecular zones, we predict a sharp drop in the dust temperature, in agreement with the bimodal dust color temperatures observed in the two zones. In the outer molecular shell, the dust temperature drops to nearly the blackbody temperature, and becomes independent of grain size because of self-shielding at shorter UV wavelengths and increased heating at longer wavelengths. This relaxes constraints on large grain sizes suggested by near-blackbody color temperatures. Finally, from the strength of infrared [Fe II] emission in the inner shell we find that the gas-phase Fe abundance is roughly solar. This is astonishing in such a dusty object, where one normally expects gaseous iron to be depleted by 2 orders of magnitude.

Subject headings: circumstellar matter — dust, extinction — ISM: individual (Homunculus nebula) — stars: individual (η Carinae) — stars: winds, outflows

1. INTRODUCTION

The bipolar Homunculus Nebula surrounding η Carinae offers an unusually well constrained laboratory to study a wide array of physical processes in the interstellar medium. The distance, size, shape, orientation, and structure of the nebula are all known (Smith 2006; Davidson et al. 2001), as are its expansion velocity and age (Morse et al. 2001; Currie & Dowling 1999; Smith & Gehrz 1998). Ionized ejecta outside the Homunculus indicate nitrogen-rich gas (Davidson et al. 1986; Dufour et al. 1999; Smith & Morse 2004), and the recent detection of ammonia in the Homunculus suggests that it too is N-rich (Smith et al. 2006). The Homunculus itself is mostly neutral, since the star's dense wind extinguishes nearly all of the Lyman continuum produced by the system. This means that familiar temperature and density diagnostics of low-density ionized gas in H II regions (e.g., Osterbrock & Ferland 2006) cannot be used here. At UV/visual wavelengths the Homunculus is seen mainly in reflection. The dust that absorbs and scatters this light acts as a calorimeter by re-emitting the absorbed luminosity in the infrared (IR), providing us with a practical and accurate measure of the bolometric luminosity of the central source (e.g., Smith et al. 2003b; Cox et al. 1995; Hackwell et al. 1986; Davidson 1971; Pagel 1969; Westphal & Neugebauer 1969). Despite these constraints, η Car's nebula is such a bright and complex object that it leaves no shortage of observational puzzles. These can sometimes make it difficult to see the trees for the forest.

Relevant physical conditions in the Homunculus Nebula can be constrained if we understand the origin of the distinct double-shell structure in the walls of the nebula. These layers manifest themselves in three independent ways that have been clearly observed. First, high-resolution thermal-IR images reveal a stratification in the dust color temperature, with a thin outer shell at $\sim$140 K, and a warmer, thicker inner zone with a color temperature of $\sim$200 K (Smith et al. 2003b). Second, near-IR spectra show an outer skin of H_2, and an inner shell in tracers of dense, low-ionization atomic gas such as collisionally excited lines of [Fe II] (Smith 2002a, 2006). These two layers are segregated from one another. Third, the two distinct shells can be seen at different radial velocities in UV absorption profiles along our line of sight to the star (Gull et al. 2005, 2006; Nielsen et al. 2005). The outer molecular layer is also detected in UV absorption lines of CH and OH (Verner et al. 2005), and the inner layer is also seen in visual-wavelength emission lines such as [Ni II] and [Fe II], plus faint emission of Hα and [N II] (Davidson et al. 2001; Hillier & Allen 1992; Allen & Hillier 1993; Smith et al. 2003a). A detailed account of this structure was given recently by Smith (2006, hereafter Paper I).

It is this pronounced double-shell structure that we aim to reproduce in the model presented here. We are particularly interested in the physical conditions that allow H_2 to form and survive

---

[2] Hubble Fellow.
[3] Current address: Astronomy Department, University of California, Berkeley CA; nathans@astro.berkeley.edu.

in such a thin layer. So far, η Carinae is the only luminous blue variable (LBV) known to be surrounded by molecular gas in its own ejecta, while nearly all LBV nebulae exhibit bright near-IR emission of [Fe II] (Smith 2002b; Smith & Hartigan 2006). The H_2 is probably a consequence of the extreme youth and high density of the nebula. New observations presented in Paper I, obtained with the Phoenix spectrograph on the Gemini South telescope, have shown the H_2 layer to be surprisingly thin (only a few per cent of the radius) and uniformly so, despite the fact that it traces a wide range of different radii at various latitudes in the bipolar nebula. This hints that the near-IR H_2 emission arises at the inside surface of an optically thick shell, which absorbs the remainder of whatever far-UV (FUV) radiation penetrates the inner [Fe II]-emitting zone. By varying the density in this outer shell, we can test what physical density permits H_2 to survive. This density constraint, in turn, provides an independent measure of the mass of the Homunculus because the geometric thickness of the shell is known. The total mass is thought to be at least 12 $M_\odot$ derived from IR dust observations (Smith et al. 2003b).[4] Here we are fine-tuning an earlier uniform-density shell model for the physical conditions in the Homunculus (Ferland et al. 2005) in order to account for the observed thin structure of the H_2 layer.

2. ADOPTED PARAMETERS IN CLOUDY

We simulate the conditions within the nebula using the development version of CLOUDY, last described by Ferland et al. (1998). The incident stellar continuum is represented by an interpolated 20,000 K CoStar atmosphere with a total luminosity of 5×10^6 $L_\odot$. To account for the hard X-rays from the colliding wind binary system, we add a high-energy component corresponding to a 3×10^6 K blackbody with a luminosity of 30 $L_\odot$ (e.g., Corcoran et al. 2001). The lack of a prominent H II region shows that few hydrogen-ionizing photons strike the inner edge of the nebula, most likely due to absorption by the stellar wind. Therefore, we extinguish the net continuum by photoelectric absorption from a neutral hydrogen layer of 10^{21} cm^{-2} to account for this. Some high-energy photons are transmitted and they help drive the chemistry. We also include the galactic background cosmic-ray ionization rate, although the actual ionization rate may be higher if radiative nuclei are present. Cosmic rays have effects that are similar to X-rays, providing ionization that helps drive the chemistry. We adopt solar gas-phase abundances except for the following: He/H = 0.4, [C/H] = −4.4, [N/H] = −2.82, and [O/H] = −4.12. The gas : dust mass ratio was set to the normal ISM value of 100, and we adopted silicate grains rather than graphitic grains because the 2175 Å absorption feature is absent in observations (e.g., Hillier et al. 2006) and the 10 μm silicate emission feature is strong (see, however, Chesneau et al. 2005).

We chose the nebular geometry to be a thick shell separated into two radial zones, where the concentric shells are permitted to have different densities. Table 1 gives our adopted geometric and physical properties of the double-shell structure. The inner shell (zone 1) has lower density and is geometrically thicker, corresponding to the gas traced by infrared [Fe II] lines and warm $\sim$200 K dust. The outer shell (zone 2) is very thin and corresponds to the material traced by H_2 emission and cooler $\sim$140 K dust. The outer edge of the inner shell is directly in contact with the inner surface of the outer shell. We calculated the physical conditions in these two zones separately in CLOUDY, using the *transmitted* continuum at the outside of zone 1 as the *incident* continuum for

[4] Note that the gas : dust mass ratio of 100 assumed in deriving this mass might be too low, due to the depletion of C and O in the ejecta. Also, η Car's grains may have unusual composition (Chesneau et al. 2005).

TABLE 1
CALCULATION OF THE DOUBLE-SHELL STRUCTURE AT THE POLE

Parameter	Zone 1	Zone 2	Zone 2	Zone 2	Zone 2	Zone 2
		Input Parameters				
log R_{in} (cm)	17.255	17.398	17.398	17.398	17.398	17.398
log R_{out} (cm)	17.398	17.415	17.415	17.415	17.415	17.415
log ΔR (cm)	16.845	16.0	16.0	16.0	16.0	16.0
log n_H (cm^{-3})	5.5	7.0	6.7	6.5	6.3	6.0
log N_H (cm^{-2})	22.35	23.0	22.7	22.5	22.3	22.0
M_{total}[a] ($M_\odot$)	1	33	16	11	7.5	3.7
Filling factor	0.5	0.9	0.9	0.9	0.9	0.9
		Calculated Parameters				
log n_e (cm^{-3})	3.7	4.5	4.35	4.26	4.2	4.0
T_e (K)	170	118	142	169	190	191
Fe$^+$/Fe	1.0	2(-4)	0.97	1.0	1.0	1.0
$n(H^+)/n_H$	0.016	2(−12)	2(−3)	3(−3)	3(−3)	1(−4)
max $2n(H_2)/n_H$	5(−10)	1.0	1.0	0.99	0.42	2(−4)
D $2n(H_2)/n_H$ = 0.5	. . .	0.15	0.36	0.61	. . .	. . .
D $2n(H_2)/n_H$ = 0.99	. . .	0.41	0.88	. . .	. . .	. . .
A_V (mag)	1.1	8.9	4.5	2.8	1.8	0.9

NOTES.—The first seven rows are prescribed inputs. The results of the calculation in the remaining rows are example values at roughly the midpoints in each zone. The value of n_H corresponds to the total hydrogen density $n(H_2+H^0+H^+)$. In the last two rows, the value of D gives the fractional depth into the shell at which the H_2 fraction reaches either 50 or 99%.

[a] This is the total mass assuming that the volume of the bipolar Homunculus (Paper I) is filled with the shell's density. This mass will be different from that for an equivalent spherical shell.

zone 2. Although the shells were calculated using spherical symmetry in CLOUDY, they are meant to approximate the observed properties of the nebula roughly along our sight line through the polar region of the bipolar lobes. The equatorial region of the nebula with much smaller radii was modeled separately (see below). The inner and outer radii for the two zones were taken directly from observations (Paper I) and are not free parameters.

Our goal is to investigate the densities in these two zones, to answer the following questions: (1) What is the density in zone 1 that is consistent with the observed n_e value of $\lesssim 10^4$ cm^{-3} (Smith 2002a) and permits significant FUV radiation to fully penetrate the shell, causing iron to remain as Fe$^+$ throughout? (2) What is the minimum density in zone 2 that allows hydrogen to become predominantly molecular, and iron to recombine to Fe^0? The most important free parameters here are therefore the value of n_H chosen for each zone, but other factors, such as the gas : dust mass ratio and the filling factor, play roles as well. The main determining factor in whether or not H_2 can survive in zone 2 is the attenuation of FUV radiation in the Lyman and Werner bands by the total column density of gas and dust in both zones. Based on spatially resolved infrared [Fe II] spectra (Paper I), we adopt a volume filling factor of 0.5 in zone 1. From similar H_2 spectra and the size scales of structures seen in *Hubble Space Telescope* images (Morse et al. 1998) we adopt a filling factor of 0.9 for the thin outer shell in zone 2. A fraction of 0.9 also matches the fraction of the total stellar luminosity absorbed by dust grains that is reemitted in the IR, while $\sim$10% of the starlight escapes at near-UV and visual wavelengths.

Finally, we note that we have ignored the possible influence of the Little Homunculus (Ishibashi et al. 2003). This inner nebula has a much lower mass—a few percent of the Homunculus (Smith 2005)—and is apparently clumpy on large scales, allowing both radiation and wind to leak through. Thus, its influence should be minimal, absorbing whatever small amount of Lyman continuum
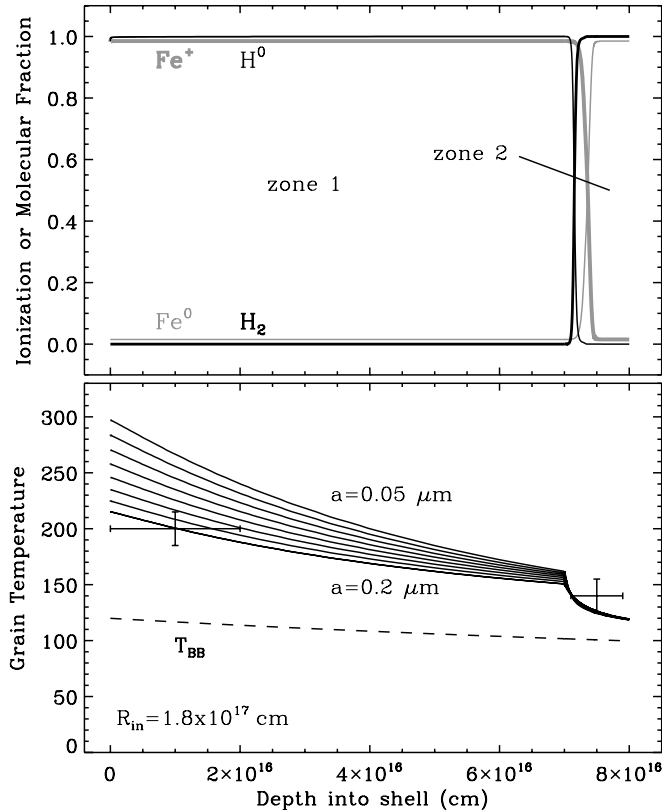
FIG. 1.—Variation of observable physical properties throughout the thick shell, where the left edge marks the inner radius of the inner shell (zone 1), and the right edge marks the outer surface of the Homunculus. The top panel shows the variation in the relative fraction of atomic/molecular hydrogen (*thin/thick black lines*), as well as the neutral and singly ionized Fe fractions (*thin/thick gray lines*). Here we show the model with $n_H = 10^7$ cm^{-3} in zone 2. The bottom panel shows the grain temperature at the same locations for a range of different grain radii a, where the dashed curve is the equilibrium blackbody temperature. The error bars in the bottom panel show observed grain color temperatures for the inner and outer shells (from Smith et al. 2003b). The physical parameters in the model are summarized in Table 1.

radiation may escape the dense stellar wind, causing strong variability in the radio continuum (Duncan et al. 1997).

3. RESULTS ALONG OUR SIGHT LINE

Figure 1 shows the results of a CLOUDY calculation matched to observations of the polar lobes of the Homunculus (Paper I). The transition between zones 1 and 2 is sudden at a depth of a little more than 7×10^{16} cm, showing a thick inner zone traced by [Fe II] and a very thin outer shell seen in H$_2$ emission. In order to reproduce this sharp transition, the simulation required a strong density increase of a factor of 15–30 from zone 1 to 2.

Throughout zone 1, hydrogen remains fully atomic, while Fe is singly ionized (representative values about halfway through zone 1 give an H$_2$ fraction of 5×10^{-10} and a neutral Fe fraction of 2×10^{-6}). The electron density from infrared [Fe II] line ratios in zone 1 is $n_e \lesssim 10^4$ cm^{-3} (Smith 2002a). To match this constraint, the hydrogen density in zone 1 was set to $10^{5.5}$ cm^{-3}, since n_e/n_H was only about 3% at this distance from the star. Only 1%–2% of the hydrogen was ionized at the innermost edge of zone 1, probably through Balmer continuum ionization from the 2 s level. This may account for the faint Hα emission there (Smith et al. 2003a; Davidson et al. 2001), as well as faint radio continuum (Duncan et al. 1997). In both zones 1 and 2, heating of the gas was
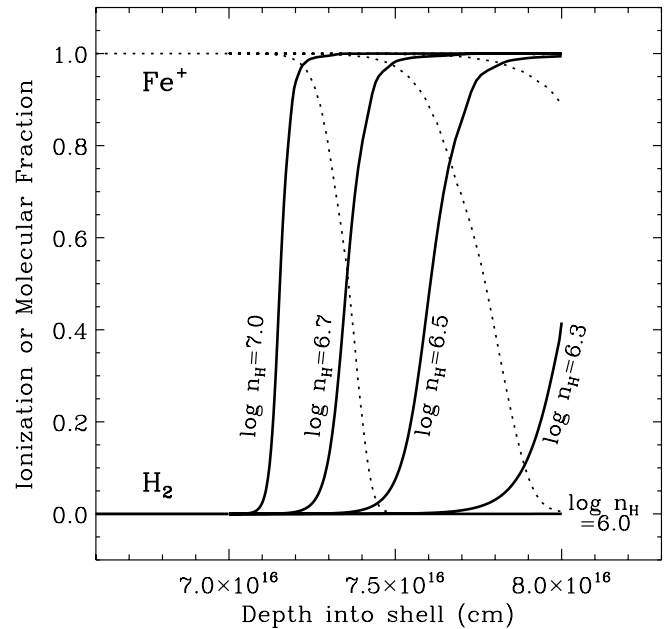

FIG. 2.—Detail of Fig. 1, concentrating on zone 2, showing the transition to molecular hydrogen for several different values of the density in zone 2 (see Table 1). The molecular gas fraction is shown by solid curves, while the ionization fraction of Fe$^+$ is shown by the dotted curves.

dominated ($\gtrsim$90%) by grain-gas photoelectric heating, whereas direct heating by line absorption was minimal.

To investigate the formation of H$_2$ and the recombination of Fe in zone 2 we considered several different values for the hydrogen density, and we discuss a few representative values here: $n_H = 10^6$, $10^{6.3}$, $10^{6.5}$, $10^{6.7}$, and 10^7 cm^{-3}. Table 1 lists the properties in zone 2 at these various densities, and Figure 2 gives a detailed view of the transition to molecular gas for each of these adopted densities.

With $n_H = 10^6$ cm^{-3}, we found that H$_2$ did not form at all, with H remaining fully atomic and Fe remaining singly ionized throughout zone 2. When the density was raised to 2×10^6 cm^{-3}, H$_2$ did begin to form at the outer edge of zone 2; the molecular fraction reached a maximum of about 40% at the outermost edge (Fig. 2). However, Fe remained singly ionized throughout zone 2 at this density. This is not in agreement with observations, since Fe I absorption is seen from zone 2 in UV spectra (Nielsen et al. 2005), so the density must be higher than 2×10^6 cm^{-3}. At a density of 3×10^6 cm^{-3}, hydrogen became 99% molecular at the outer edge of the shell (Fig. 2), but Fe$^+$ still did not recombine to Fe^0.

Observations suggest that H$_2$ should form and the recombination of Fe should occur *early* in zone 2, especially at the remote polar regions where the radiation field is weaker than at other latitudes. This condition is met only for higher hydrogen densities around $10^{6.7}$ to 10^7 cm^{-3} (Fig. 2). At a depth of only about 10^{15} cm into zone 2 (10%–20% of the way through the layer), the H$_2$ fraction begins to rise sharply. This is because its destruction rate collapses as UV radiation in the Lyman and Werner bands becomes optically thick and is extinguished by the much higher column density of gas and dust encountered here. Once molecules begin to form, the transition is rapid. Hydrogen remains fully molecular throughout the rest of zone 2, while Fe$^+$ does finally recombine. The Fe$^+$/Fe^0 transition occurs at a slightly larger depth than the atomic/molecular hydrogen transition, because Fe^0 can still be ionized by Balmer continuum photons with wavelengths longer than the Lyman-Werner bands. The hydrogen density is probably not much above 10^7 cm^{-3}, because then the H$_2$ shell

would be thicker than observed, and the extinction to the star would be unreasonably high.

The bottom panel of Figure 1 shows the dust temperature for various grain radii at a range of depths through the shell. In zone 1, we see that only the largest grains with radii $a \gtrsim 0.2$ μm can match the observed dust color temperatures. The transition to higher densities at the beginning of zone 2 is accompanied by a sharp drop in the grain temperature, as observed in mid-IR images (Smith et al. 2003b). This sharp drop to lower grain temperatures only occurred for the highest density models with $n_H = 10^{6.7}$ to $10^{7.0}$ cm^{-3} in zone 2. The grain temperature in zone 2 appears to be independent of grain size. This is perhaps because much of the short-wavelength FUV radiation has been extinguished and the grains are heated predominantly by radiation at near-UV, visual, and IR wavelengths instead, where the absorption efficiency is less sensitive to grain size (e.g., Draine 2003). In this case, grain-gas photoelectric heating will drop as well. In fact, we see that the grain temperature eventually drops to within 20 K of the equilibrium blackbody temperature T_{BB} (*dashed line*), independent of grain radius. The fact that the temperature in zone 2 is nearly independent of grain size is interesting, because it contradicts long-held conventional wisdom. The observed near-blackbody color temperature has often been taken as an indication that the grains have radii of 1–2 μm (Smith et al. 1998, 2003b; Polomski et al. 1999; Hackwell et al. 1986; Mitchel et al. 1983). However, Figure 1 indicates that grains this large may not be necessary to explain the grain temperature in zone 2 after all (although some large grains are still needed for the nearly gray extinction; Rodgers 1971; Hillier 2006; Whitelock et al. 1983). In particular, a population that includes *both* large and small grains is evidently allowed in zone 2.

The visual extinction through zone 1 is only ~1 mag, compared to about 4.5–9 mag for zone 2 (Table 1). Thus, the thin outer H_2 shell dominates the visual extinction, the total infrared luminosity, and also the scattered light seen in visual-wavelength images and hard X-rays (Corcoran et al. 2004). This is why model shapes for the Homunculus derived from [Fe II] or [Ni II] emission from zone 1 (Davidson et al. 2001; Allen & Hillier 1993) are too small compared to images, whereas model shapes derived from H_2 emission have the correct apparent size (Paper I).

The stellar continuum that illuminates the nebula is strongly reprocessed by the inner region before it reaches the denser outer zone. Figure 3 shows the stellar continuum (*the smoother dotted line*) that is incident on the inner nebula. The gray solid line with many spectral emission features is the net emission that emerges from the inner region and goes on to irradiate the molecular gas in zone 2. This continuum is a combination of the attenuated incident continuum plus reprocessed emission from the inner nebula. The UV continuum has been heavily absorbed by dust within the inner region. Thermal dust emission dominates the infrared continuum, and the dust is warm enough for the 10 μm silicate feature to come into emission. Many emission lines, mainly atomic and singly ionized species, are formed in the inner region. The major effect of this reprocessed continuum will be on dust in the outer nebula. Much of the incident UV continuum has been converted into thermal-IR emission already. The UV is the most effective in photoelectrically heating gas, so the outer nebula is cooler as a result of the absence of this light, as noted earlier. The very strong infrared continuum heats the outer nebula indirectly, by first heating the dust, which then shares its energy with the gas as the result of gas-dust collisions.

The emergent spectrum from zone 2 with $n_H = 10^{6.7}$ cm^{-3} is shown with the solid black line in Figure 3. As expected, the thermal-IR continuum is shifted toward longer wavelengths
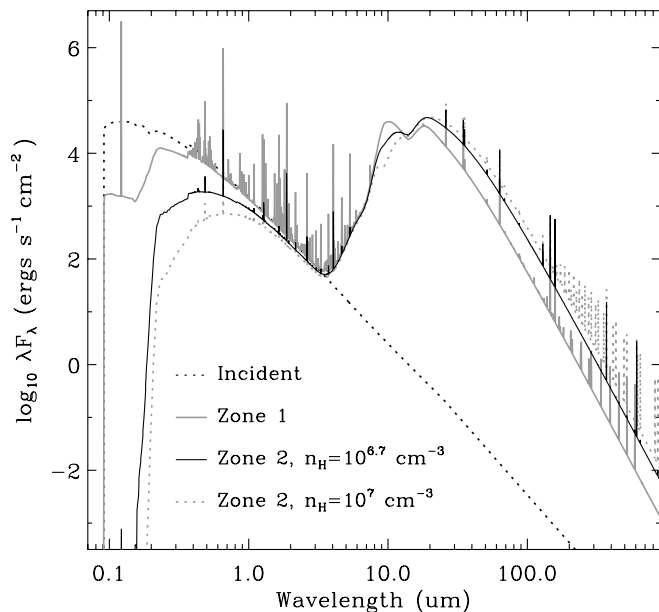

Fig. 3.—Incident continuum (*dashed line*) and emergent spectra from zone 1 (*solid gray line*) and zone 2 for the model in the polar lobes. For zone 2 we show the emergent spectrum for both plausible hydrogen densities of $10^{6.7}$ cm^{-3} (*solid black line*) and for 10^7 cm^{-3} (*dashed gray line*).

because of the cooler dust, and the UV/visual light is more severely attenuated than for zone 1. Interestingly, when we compare the spectrum from zone 1 alone to the emergent spectrum from zone 2 (which includes the emergent spectrum of zone 1 that passes through zone 2), we see that the 10 μm silicate feature has a different shape—the silicate profile from zone 2 is somewhat muffled, indicating that the emission is beginning to turn optically thick. In fact, when the density is increased to $n_H = 10^7$ cm^{-3} in zone 2 (*dashed gray line*) the silicate feature turns clearly to self-absorption. This trend in the silicate profile shape has two important implications. First, when the emission begins to turn optically thick, the silicate profile appears wider and flatter, and the peak moves toward longer wavelengths. This effect will modify the required contribution from other grain species such as corrundum (see Chesneau et al. 2005). Second, the strong silicate feature observed in η Car's mid-IR spectrum may indicate that densities of $n_H = 10^7$ cm^{-3} are too high (although the effects of clumping are an issue). If densities near our lower bound $n_H = 10^{6.7}$ cm^{-3} are preferred, then a total mass of the Homunculus near 16 $M_\odot$ is favored over a much larger value of ~30 $M_\odot$ (see § 5.1). This is, perhaps, a relief. High spatial resolution spectroscopy of the silicate profile in the Homunculus could provide a powerful and independent constraint on the density and total mass of the nebula.

4. CONDITIONS IN THE EQUATORIAL PLANE

Near-infrared H_2 emission is seen at all latitudes in the Homunculus (Paper I), even though the distance from the star changes by an order of magnitude. In the side walls of the polar lobes at midlatitudes, the oblique incident angle of the radiation (i.e., "seasons") will mitigate the stronger radiation field at closer radii to the central star, but this geometric advantage disappears for the molecular gas at the pinched waist of the nebula. Thus, we also investigate the physical conditions in the equatorial plane of the Homunculus, where H_2 is seen nearest to the star. The equatorial model was identical to the polar lobe/line-of-sight model, except that the radii and thicknesses of zones 1 and 2 were

TABLE 2
DOUBLE-SHELL STRUCTURE AT THE EQUATOR

Parameter	Zone 1	Zone 2
Input Parameters		
$\log R_{in}$ (cm).........................	16.0	16.498
$\log R_{out}$ (cm)........................	16.498	16.618
$\log \Delta R$ (cm)........................	16.332	16.0
$\log n_{H}$ (cm^{-3})......................	6.3	7.0
$\log N_{H}$ (cm^{-2})......................	22.63	23.0
Filling factor	0.5	0.9
Calculated Parameters		
$\log n_{e}$ (cm^{-3})	6.2	5.7
T_{e} (K)...................................	610	170
Fe^{+}/Fe	0.82–1	4(−4)
$n(H^{+})/n_{H}$.............................	0.74	2(−12)
$\max 2 \times n(H_{2})/n_{H}$	2(−13)	1.0

NOTES.—The first six rows are prescribed inputs. The results of the calculation in the remaining rows are example values at roughly the midpoints in each zone. The value of n_{H} corresponds to the total hydrogen density $n(H_{2} + H^{0} + H^{+})$.

adjusted to match observations (Paper I),[5] and the density in zone 1 was increased. The equatorial model is summarized in Table 2.

Figure 4 shows the results of a CLOUDY calculation matched to observations of the radial stratification in the equatorial plane of the Homunculus (Paper I). The inner radius is set approximately equal to the distance between the star and the Weigelt knots, which is 0″2 to 0″3 (Smith et al. 2004; Dorland et al. 2004), or roughly 10^{16} cm if we correct for the 41° inclination angle (Paper I; Davidson et al. 2001). In order to match observed electron densities of $>10^{6}$ cm^{-3} in the Weigelt knots and other bright equatorial ejecta (Smith 2002a; Hamann et al. 1999, 1994; Davidson et al. 1995), the simulations required a hydrogen density of about $n_{H} = 2 \times 10^{6}$ cm^{-3} or more.[6] This was also the highest density that allowed H to remain predominantly atomic and Fe to remain as Fe^{+} throughout zone 1. Even though the material is much closer to the star and feels a much stronger radiation field than in the polar model, $n_{H} \simeq 10^{7}$ cm^{-3} in zone 2 was still sufficient to allow a sharp transition to molecular hydrogen and neutral Fe.

Unlike the polar model, the inner edge of zone 1 experienced a more substantial H^{+} fraction of ~75%, while ~20% of the iron was ionized to Fe^{++}. This ionization occurs despite the fact that, aside from hard X-rays (Corcoran et al. 2001), we did not include radiation from a hot companion star in our calculation. Throughout most of zone 1, the typical molecular hydrogen fraction was of order 10^{-13}, while the neutral Fe fraction was typically 10^{-6}.

The bottom panel of Figure 4 shows the dust temperature for grains in the equatorial model. In zone 1, the predicted dust temperatures greatly exceed observational constraints on the color temperature for most grain sizes. The hottest extended dust in the core of the Homunculus (associated with the Weigelt knots and more distant ejecta) is about 550 K (Smith et al. 2003b; Chesneau et al. 2005). This is marginally consistent with $a = 0.2$ μm grains

---

[5] Note, however, that the radius at the equator depends on azimuth, due to large-scale irregular structures in the inner torus (Smith et al. 2002; Chesneau et al. 2005; Paper I).

[6] This is only the average density. In fact, some clumps, such as the cores of the Weigelt knots, may have much higher peak densities of 10^{8} to 10^{9} cm^{-3} (Hamann et al. 1999).
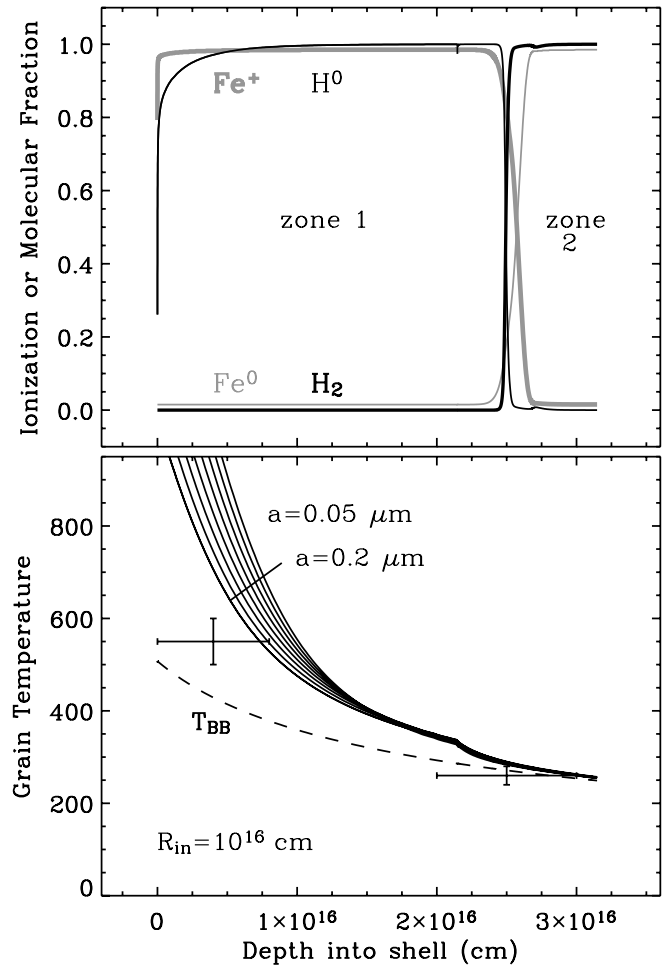

FIG. 4.—Same as Fig. 1, but showing the model for the ionization/molecular fraction and dust temperature in the equatorial plane of the Homunculus (see Table 2).
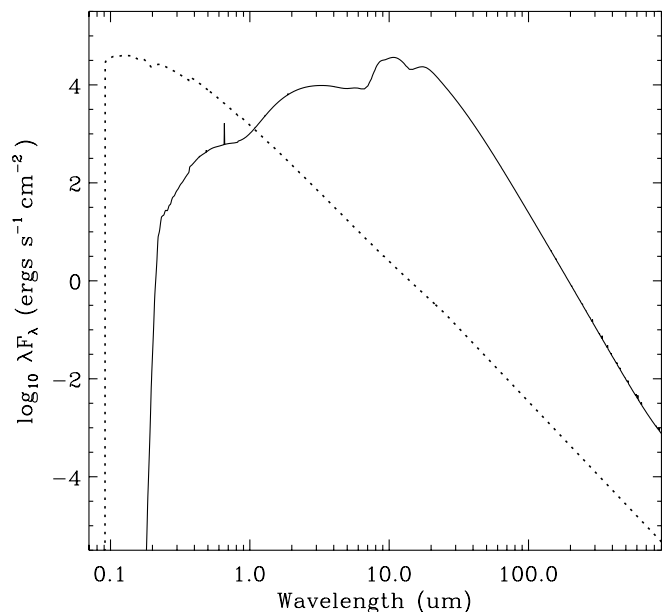

FIG. 5.—Incident (*dotted line*) and transmitted (*solid line*) continuum radiation for the model in the equatorial plane. This transmitted continuum radiation escapes to illuminate gas and dust at larger radii in the equatorial skirt, such as the so-called strontium filament.

within observational uncertainty, but the observed temperatures would be more consistent with significantly larger grains. The transition to lower dust temperature at the boundary between zones 1 and 2 is not as stark as in the polar model, but like the polar model, the grain temperature in zone 2 drops and becomes insensitive to grain size (Fig. 4). Here it fully reaches temperatures as low as the equilibrium blackbody temperature T_{BB}.

Figure 5 shows the incident (*dotted line*) and transmitted energy distributions for the equatorial model. The transmitted radiation is that which escapes from the outer boundary of zone 2. This emission at the equator is of particular interest, as it illuminates material in the equatorial skirt at larger radii. Some of that equatorial gas has peculiar spectral properties, such as the so-called "strontium filament" (Hartman et al. 2004; Zethson et al. 2001; Bautista et al. 2006, 2002), the very bright and possibly fluorescent [Ni II] $\lambda 7379$ emission (Davidson et al. 2001), and He I $\lambda 10830$ emission (Smith 2002a). In Figure 5 we see that radiation shortward of 2000 Å is severely attenuated, while near-UV radiation beyond this limit remains strong.

5. DISCUSSION

5.1. Threshold Density for H_2 Survival

Our most important observational constraint on the density in the polar lobes is that molecular hydrogen is able to survive and Fe becomes neutral, even though they are within only 0.1 pc of the most luminous hot supergiant in our Galaxy. Furthermore, both of these conditions should be met in the polar model of zone 2 with some room to spare, since H_2 emission is seen to be fairly uniform at all latitudes, including lower latitudes closer to the equator (and closer to the star), where the radiation field is stronger. As we have discussed above, these constraints are only met for high densities of $n_H = 10^{6.7}$–$10^{7.0}$ cm^{-3} in zone 2.

From the thermal-IR spectral energy distribution and conservative assumptions, Smith et al. (2003b) derived a lower limit to the total mass of the Homunculus of about 12.5 $M_\odot$ (about 11 $M_\odot$ in the cool 140 K shell, and 1.5 $M_\odot$ in the warmer inner shell). If this mass of cool dust were spread evenly over the volume of the H_2 shell inferred observationally, the density would be at least $n_H = 10^{6.5}$ cm^{-3} in zone 2 (Paper I). However, our CLOUDY calculations show that even higher densities are likely, as noted above. These higher average densities distributed over the same volume would imply a total gas mass for the Homunculus in the range of roughly 15–35 $M_\odot$. Thus, our study confirms the large mass of the Homunculus deduced from IR observations of dust, but uses an independent method sensitive to the gas density. It also confirms that previous IR estimates were indeed lower limits to the total mass. We also find that 35 $M_\odot$ is an upper limit to the mass, since for densities much higher than 10^7 cm^{-3}, the transition to molecular gas would occur earlier and the H_2 shell would be thicker than observed.

Caveats: Although our mass estimate is sensitive to the gas density, it is not completely independent of the gas : dust ratio, since dust helps attenuate the UV radiation in the Lyman-Werner bands that destroys H_2, and grains act as a catalyst by providing a surface for H_2 formation. However, like mass estimates from thermal-IR dust emission, these are probably underestimates if they are wrong.

5.2. Dust Temperature and Grain Properties

Our CLOUDY calculations were tuned to match the observed structure in IR lines of H_2 and [Fe II], but they naturally reproduce the bimodal stratification of the observed dust color temperature as well. High-resolution thermal-IR images show a thick inner

shell at $\sim$200 K and a thin outer shell at $\sim$140 K (Smith et al. 2003b), where the cooler dust color temperatures are coincident with the outer H_2 shell. This is clearly reproduced in our model (Fig. 1).

Our earlier simulations with CLOUDY used a uniform density of 10^6 cm^{-3} throughout a thick shell (Ferland et al. 2005) and were able to reproduce a transition from H to H_2 and Fe$^+$ to Fe^0 at some point within the shell, *but in that model a sharp drop in dust temperature did not occur at the same position as the onset of H_2.* Instead, in the constant-density thick-shell model, the dust temperature began to drop immediately at the inner radius of the shell and continued smoothly thereafter. Therefore, the observed sharp transition from a geometrically thick zone of $\sim$200 K to a very thin layer of $\sim$140 K dust coincident with the onset of the thin H_2 shell (Fig. 1) gives a robust and independent confirmation that a sharp density contrast between the two zones is indeed required.

Because of the strong density increase of a factor of 15–30 from zone 1 to zone 2, the model also successfully reproduced the relative contributions to the total mass observed in each component. Fits to the IR spectral energy distribution (Smith et al. 2003b) show that the 200 K dust in the inner shell only contains about 10% of the total mass in the nebula, while the rest of the mass resides in the thin outer shell at 140 K. Because the outer shell is so thin, it must be much denser in order to have a higher total mass. The relative masses for the inner ($\sim$1 $M_\odot$) and outer (16–33 $M_\odot$) shells in Table 1 agree with these observational constraints. By stark contrast, a uniform-density thick shell would have much more mass in the [Fe II] zone.

Interestingly, the radial behavior of the dust temperature brings into question long-held notions about the grain properties. Several authors have noted that the low dust color temperatures at thermal-IR wavelengths are close to the equilibrium blackbody temperatures at those radii, suggesting large grain sizes above $a \simeq 1\,\mu$m (Mitchell et al. 1983; Mitchell & Robinson 1986; Hackwell et al. 1986; Robinson et al. 1987; Apruzese 1975; Smith et al. 1998; Smith et al. 2003b; Polomski et al. 1999).[7] In contrast, we find that the dust temperature in the outer layer is *independent of grain size* (Figs. 1 and 4), and approaches the equilibrium blackbody temperature even for small grains. The material becomes optically thick and severely attenuates the UV radiation, leaving the burden of energy balance to heating by longer wavelength radiation. At longer wavelengths, the difference between absorption efficiency and the thermal-IR emissivity is smaller, allowing small and large grains to maintain similar temperatures. The dust temperature never gets below the equilibrium blackbody temperature in our calculations. Therefore, the very low dust temperature of 110 K that Morris et al. (1999) deduced from fits to the far-IR spectral energy distribution is probably too low, especially at the small radii in the equator suggested by those authors.

Although the temperature is apparently independent of grain size in zone 2, very small grains are not permitted in zone 1 because corresponding high temperatures are not seen there. The color temperature in zone 1 is about $\sim$200 K, which would be consistent with grains of radius $a \gtrsim 0.2\,\mu$m. Thus, our calculations relax but do not eliminate the constraints on large grain size posed by the low observed dust temperatures in the Homunculus. Allowing the presence of somewhat smaller grains may be relevant to the high degree of polarization (Thackeray 1961; Visvanathan

---

[7] Note, however, that Mitchell et al.'s suggestion of very large grains was also motivated in part by the very broad 10 μm silicate emission feature, but Chesneau et al. (2005), Mitchell & Robinson (1978), and Hyland et al. (1979) have suggested that this may be due to a partial contribution from other grain emission features such as corrundum.

1967; Warren-Smith et al. 1979; Meaburn et al. 1987, 1993; Walsh & Ageorges 2000) and the unusual scattering properties of the Homunculus seen in high-resolution polarization imaging (Schulte-Ladbeck et al. 1999).

5.3. *Bright* [Fe II] *Emission from the Inner Shell and the Gas-phase Iron Abundance*

An accurate model for zone 1 determines the radiation field that penetrates it to illuminate the outer H_2 shell (Fig. 3), but the inner shell is interesting in its own right because of the physical conditions that give rise to the extraordinarily bright infrared [Fe II] emission seen there (Paper I). These bright infrared [Fe II] emission lines are a common feature of other LBV nebulae (Smith 2002b; Smith & Hartigan 2006), which is in contrast to the outer H_2 shell that seems to make η Car unique among hot luminous stars.

To investigate this bright [Fe II] emission in detail, we ran CLOUDY using the more sophisticated large Fe atom. This predicts the strength of numerous Fe lines, including the distinct [Fe II] $(a^6D–a^4D)$ and $(a^4F–a^4D)$ transitions in the 1–2 μm region. For example, with solar Fe abundance, our CLOUDY model for zone 1 predicts a total luminosity for [Fe II] $\lambda16435$ of about 65 $L_\odot$. This line has been observed extensively in η Car in both moderate- and high-resolution spectra (Smith 2002a; Paper I), and exhibits an average brightness in the polar lobes of about 2×10^{-12} ergs s^{-1} cm^{-2} arcsec^{-2} (although the local value is highly spatially dependent). Integrating this over the roughly 140–150 arcsec^2 projected area of the Homunculus would indicate a total flux in this line of 3×10^{-10} ergs s^{-1} cm^{-2} (excluding the bright [Fe II] contribution from the Little Homunculus; Smith 2005). This corresponds to a total observed [Fe II] $\lambda16435$ luminosity of about 40–50 $L_\odot$. The agreement between our model's predicted luminosity of 65 $L_\odot$ and the observed value of $\sim$45 $L_\odot$ in this same line is remarkable, considering that the bipolar Homunculus has a somewhat smaller projected area on the sky than the equivalent-radius spherical shell in CLOUDY. This match indicates that the gas-phase Fe abundance is indeed roughly solar in zone 1.

A solar gas-phase Fe abundance here is actually quite astonishing. In dusty regions of the ISM, the abundance of Fe is normally depleted by 2 orders of magnitude due to the formation of Fe-bearing grains (e.g., Shields 1975). We do not expect the overall dust-to-gas ratio in zone 1 to be unusually low, since the mass inferred for the gas from the observed electron density agrees with the mass measured from the 200 K dust component that occupies the same region (uncertainties of a factor of 2 are likely, but not factors of 100). Therefore, some process has selectively destroyed Fe-bearing grains *without* destroying the remaining grain population, or some mechanism has specifically inhibited the formation of Fe-bearing grains.

Shock speeds $\gtrsim$80 km s^{-1} can destroy iron grains and release the corresponding atomic Fe into the gas phase. While we see no spectroscopic evidence for such fast shocks in the polar lobes today, shocks of this speed may have been active earlier in the life of the Homunculus. If such shocks destroyed the Fe-bearing grains early on, they may have been released into an environment where the density was too low to reform the grains, locking Fe in the gas phase. Alternatively, the ejecta in the Homunculus are C- and O-poor, and N-rich. The low oxygen abundance may have inhibited the formation of iron oxides, which can be an important repository for storing Fe in the solid phase of the ISM. In the absence of C, O, and Fe, grains might form preferentially with Al, Mg, or Ca instead. Interestingly, mid-IR spectroscopy of the Homunculus strongly suggests the presence of Al-bearing grains such as corrundum (Mitchell & Robinson 1978; Hyland

et al. 1979; Chesneau et al. 2005). We also know that Fe is present in the gas phase in the outer H_2 shell, since Fe^0 is seen in absorption there in UV spectra (Gull et al. 2005; Nielsen et al. 2005). The existence of a region of the ISM with a high dust content and where Fe is predominantly in the gas phase has important ramifications beyond the study of η Carinae, and will be discussed elsewhere.

5.4. *Origin of the Double-Shell Structure*

We have shown that the observed double-shell structure of the Homunculus requires a strong density jump in the walls of the nebula. The observed transition from atomic to molecular gas (Paper I) and the corresponding drop in dust temperature (Smith et al. 2003b) result when FUV radiation propagating through the low-density inner zone suddenly encounters the high densities in the thin outer shell. The absorption of this UV radiation in the Lyman-Werner bands by gas and dust in the dense outer shell regulates the destruction rate of H_2, allowing the H_2 to survive. The required density contrast between these two zones is a factor of roughly 15–30.

While our CLOUDY calculations explain how the observed properties of the double-shell structure result from a strong density stratification, they do not explain the origin of the density structure itself. Since the Homunculus appears to be expanding ballistically (Smith & Gehrz 1998) and because the current stellar wind is too weak to shape the massive nebula, it is likely that this density structure was determined early. The observed stratification is reminiscent of the layered structure seen in cooling zones behind shock fronts; although this is unlikely to be occurring at the present time (Paper I), the observed density structure may be frozen-in to the ejecta from shocks that occurred during the event itself as the dense material cooled. As noted in the previous section, shocks present during an earlier epoch would also be interesting from the point of view of the gas-phase Fe abundance. The rapid cooling of this dense layer may have triggered severe thermal instabilities, which in turn, could explain the currently observed clumping and fragmentation seen in images of the Homunculus (Morse et al. 1998). Alternatively, the low-density inner zone may result from a photoevaporative flow off the inside face of the much denser outer H_2 shell, as is commonly seen in photodissociation regions at the surfaces of giant molecular clouds. Finally, an obvious possibility is that the two shells simply result from separate ejection events during the $\sim$20 yr time span of the Great Eruption. We know that this is at least plausible from the existence of the outer ejecta, the Homunculus, and the Little Homunculus, indicating that η Car has suffered multiple mass ejections (Walborn 1976; Walborn et al. 1978; Ishibashi et al. 2003; Smith 2005).

Our models that reproduce the fundamental observed structure have constrained the most basic physical properties of the Homunculus: namely, its density and temperature. These will allow further refinements to models trying to understand emission line spectra, unusual grain properties, molecular chemistry, abundances, and radiative transfer models of the appearance of η Car's nebula in images. The physical explanation for this distinct double-shell structure may have wider applications as well, especially to objects such as planetary nebulae. For example, the bipolar nebula M2-9 has a similar and pronounced double-shell structure, with a thin outer H_2 shell and an inner [Fe II] shell (Smith et al. 2005; Hora & Latter 1994). The UV radiation field of M2-9 is known to be highly asymmetric and time variable because of a central binary system (e.g., Doyle et al. 2000), so it is likely that a density jump controls the shape of the H_2 lobes, as in η Car. Our CLOUDY models for η Car would then suggest that the transition from

atomic to molecular gas in such planetary nebulae would be accompanied by a similar sharp drop in observed dust color temperature at mid-IR wavelengths, possibly insensitive to grain size as well.

5.5. *Future Evolution of the* H_2 *Shell*

Since η Car is the only LBV nebula known to have a dense H_2 shell, we must ask if this is a truly unique property of η Car itself, or if it is simply a consequence of η Car being observed at a special time so soon after its mass ejection; the Homunculus is also the *youngest* LBV nebula. We expect that in the decades immediately following the outburst, the ejecta around η Car were extremely dense and self-shielding, permitting the formation of not only dust, but also H_2 and even more complex polyatomic molecules, such as ammonia (Smith et al. 2006). The physical conditions in this early high-density epoch are of great interest. This material has since been expanding and thinning, as the observed extinction drops and the star brightens (Whitelock et al. 1983; Davidson et al. 1999; Smith et al. 2000).

Due to the high mass of the Homunculus and its relatively empty surroundings, the shell will continue to expand quasi-ballistically. Thus, the hydrogen density will drop as r^{-2}, and because of ballistic motion, roughly as t^{-2} as well. In another couple hundred years, the density in the nebula will drop below the threshold at which H_2 can survive (this may happen even sooner, since η Car resides in a giant H II region with a strong ambient UV field). Eventually, the Homunculus will become an atomic shell resembling the massive shells seen around other LBVs and LBV candidates, like the more evolved nebulae around the Pistol star (Figer et al. 1999), AG Car (Voors et al. 2000), and P Cygni (Smith & Hartigan 2006). At these later stages, the Homunculus may even overtake and mix with more distant outer ejecta (Walborn 1976), appearing as a single ringlike LBV nebula, thereby erasing the details of its eruptive history.

6. CONCLUSIONS

We have modeled the basic double-shell structure in the Homunculus, as traced most vividly by near-IR emission from [Fe II] and H_2 (Paper I). Our aim was to constrain the density that permits the survival of H_2, and thus to provide an independent constraint on the mass of the Homunculus and the physical conditions in the nebula. The main observational constraints on our CLOUDY models were the geometric thickness of each zone, the electron density in the inner [Fe II] zone, and the survival of both H_2 and Fe^0 in the thin outer zone. Our primary conclusions are as follows:

1. The hydrogen density in the outer H_2 zone is $n_H \simeq (0.5-1) \times 10^7$ cm^{-3}.

2. Using this density and the observed geometry of the nebula, the total mass is roughly 15–35 $M_\odot$, and we note reasons why the lower end of this range is favored.

3. The relative mass of gas in the two zones closely matches that derived for warm and cool dust components in the same two zones (Smith et al. 2003b). This suggests that previous assumptions of a normal gas : dust mass ratio of 100 are not wildly in error.

4. We predict a sharp drop in the dust temperature between the inner and outer zones of the double shell, as observed (Smith et al. 2003b). The temperature in the outer zone approach the equilibrium blackbody temperature independent of grain size, due to shielding of UV radiation. This relaxes constraints on the unusually large grains inferred from observed dust temperatures.

5. Even though dust formation was efficient in the ejecta of η Car, we find that the gas-phase Fe abundance is still roughly solar. One normally expects Fe to depleted by 2 orders of magnitude in dusty environments. This has occurred despite the severe depletion of C and O in the ejecta.

REFERENCES

Allen, D. A., & Hillier, D. J. 1993, Proc. Astron. Soc. Australia, 10, 338
Apruzese, J. P. 1975, ApJ, 196, 753
Bautista, M. A., Gull, T. R., Ishibashi, K., Hartman, H., & Davidson, K. 2002, MNRAS, 331, 875
Bautista, M. A., Hartman, H., Gull, T. R., Smith, N., & Lodders, K. 2006, MNRAS, 370, 1991
Chesneau, O., et al. 2005, A&A, 435, 1043
Corcoran, M. F., Ishibashi, K., Swank, J. H., & Petre, R. 2001, ApJ, 547, 1034
Corcoran, M. F., et al. 2004, ApJ, 613, 381
Cox, P., Mezger, P. G., Sievers, A., Najarro, F., Bronfmann, L., Kreysa, E., & Haslam, G. 1995, A&A, 297, 168
Currie, D. G., & Dowling, D. M. 1999, in ASP Conf. Ser. 179, η Carinae at the Millennium, ed. J. A. Morse, R. M. Humphreys, & A. Damineli (San Francisco: ASP), 72
Davidson, K. 1971, MNRAS, 154, 415
Davidson, K., et al. 1999, AJ, 118, 1777
Davidson, K., Dufour, R. J., Walborn, N. R., & Gull, T. R. 1986, ApJ, 305, 867
Davidson, K., Ebbets, D., Weigelt, G., Humphreys, R. M., Hajian, A. R., Walborn, N. R., & Rosa, M. 1995, AJ, 109, 1784
Davidson, K., Smith, N., Gull, T. R., Ishibashi, K., & Hillier, D. J. 2001, AJ, 121, 1569
Dorland, B. N., Currie, D. G., & Hajian, A. R. 2004, AJ, 127, 1052
Doyle, S., Balick, B., Corradi, R. L. M., & Schwarz, H. E. 2000, AJ, 119, 1339
Draine, B. T. 2003, ARA&A, 41, 241
Dufour, R. J., Glover, T. W., Hester, J. J., Currie, D. G., van Orsow, D., & Walter, D. K. 1999, in ASP Conf. Ser. 179, η Carinae at the Millennium, ed. J. A. Morse, R. M. Humphreys, & A. Damineli (San Francisco: ASP), 134
Duncan, R. A., White, S. M., & Lim, J. 1997, MNRAS, 290, 680

Ferland, G. J., Abel, N., Davidson, K., & Smith, N. 2005, in ASP Conf. Ser. 332, The Fate of the Most Massive Stars, ed. R. M. Humphreys & K. Z. Stanek (San Francisco: ASP), 294
Ferland, G. J., Korista, K. T., Verner, D. A., Ferguson, J. W., Kingdon, J. B., & Verner, E. M. 1998, PASP, 110, 761
Figer, D. F., Morris, M., Geballe, T. R., Rich, R. M., Serabyn, E., McLean, I. S., Puetter, R. C., & Yahil, A. 1999, ApJ, 525, 759
Gull, T. R., Vieira, G., Bruhweiler, F., Nielsen, K. E., & Danks, A. 2005, ApJ, 620, 442
Gull, T. R., Vieira Kober, G., & Nielsen, K. E. 2006, ApJS, 163, 173
Hackwell, J. A., Gehrz, R. D., & Grasdalen, G. L. 1986, ApJ, 311, 380
Hamann, F., Davidson, K., Ishibashi, K., & Gull, T. R. 1999, in ASP Conf. Ser. 179, η Carinae at the Millennium, ed. J. A. Morse, R. M. Humphreys, & A. Damineli (San Francisco: ASP), 116
Hamann, F., De Poy, D. L., Johansson, S., & Elias, J. 1994, ApJ, 422, 626
Hartman, H., Gull, T., Johansson, S., Smith, N., & the *HST* η Car Treasury Team 2004, A&A, 419, 215
Hillier, D. J. 2006, in ASP Conf. Ser., Mass Loss from Stars and Stellar Clusters, ed. A. De Koter, L. Smith, & L.B.I.M. Waters (San Francisco: ASP), in press
Hillier, D. J., & Allen, D. A. 1992, A&A, 262, 153
Hillier, D. J., et al. 2006, ApJ, 642, 1098
Hora, J. L., & Latter, W. B. 1994, ApJ, 437, 281
Hyland, A. R., Robinson, G., Mitchell, R. M., Thomas, J. A., & Becklin, E. E. 1979, ApJ, 233, 145
Ishibashi, K., et al. 2003, AJ, 125, 3222
Meaburn, J., Walsh, J. R., & Wolstencroft, R. D. 1993, A&A, 268, 283
Meaburn, J., Wolstencroft, R. D., & Walsh, J. R. 1987, A&A, 181, 333

Mitchell, R. M., & Robinson, G. 1978, ApJ, 220, 841
———. 1986, MNRAS, 222, 347
Mitchell, R. M., Robinson, G., Hyland, A. R., & Jones, T. J. 1983, ApJ, 271, 133
Morris, P. W., et al. 1999, Nature, 402, 502
Morse, J. A., Davidson, K., Bally, J., Ebbets, D., Balick, B., & Frank, A. 1998, AJ, 116, 2443
Morse, J. A., Kellogg, J. R., Bally, J., Davidson, K., Balick, B., & Ebbets, D. 2001, ApJ, 548, L207
Nielsen, K. E., Gull, T. R., & Vieira-Kober, G. 2005, ApJS, 157, 138
Osterbrock, D. E., & Ferland, G. J. 2006, Astrophysics of Gaseous Nebulae and Active Galactic Nuclei (2nd ed.; Sausalito: University Science)
Pagel, B. E. T. 1969, Astophys. Lett., 4, 221
Polomski, E. F., Telesco, C. M., Piña, R. K., & Fisher, R. S. 1999, AJ, 118, 2369
Robinson, G., Mitchell, R. M., Aitken, D. K., Briggs, G. P., & Roche, P. F. 1987, MNRAS, 227, 535
Rodgers, A. W. 1971, ApJ, 165, 665
Schulte-Ladbeck, R., Pasquali, A., Clampin, M., Nota, A., Hillier, D. J., & Lupie, O. L. 1999, AJ, 118, 1320
Shields, G. A. 1975, ApJ, 195, 475
Smith, N. 2002a, MNRAS, 337, 1252
———. 2002b, MNRAS, 336, L22
———. 2005, MNRAS, 357, 1330
———. 2006, ApJ, 644, 1151 (Paper I)
Smith, N., Balick, B., & Gehrz, R. D. 2005, AJ, 130, 853
Smith, N., Brooks, K. J., Koribalski, B., & Bally, J. 2006, ApJ, 645, L41

Smith, N., Davidson, K., Gull, T. R., Ishibashi, K., & Hillier, D. J. 2003a, ApJ, 586, 432
Smith, N., & Gehrz, R. D. 1998, AJ, 116, 823
Smith, N., Gehrz, R. D., Hinz, P. M., Hoffmann, W. F., Hora, J. L., Mamajek, E. E., & Meyer, M. R. 2003b, AJ, 125, 1458
Smith, N., Gehrz, R. D., Hinz, P. M., Hoffmann, W. F., Mamajek, E. E., Meyer, M. R., & Hora, J. L. 2002, ApJ, 567, L77
Smith, N., Gehrz, R. D., & Krautter, J. 1998, AJ, 116, 1332
Smith, N., & Hartigan, P. 2006, ApJ, 638, 1045
Smith, N., & Morse, J. A. 2004, ApJ, 605, 854
Smith, N., Morse, J. A., Davidson, K., & Humphreys, R. M. 2000, AJ, 120, 920
Smith, N., et al. 2004, ApJ, 605, 405
Thackeray, A. D. 1961, Observatory, 81, 99
Verner, E., Bruhweiler, F., Nielsen, K. E., Gull, T. R., Vieira Kober, G., & Corcoran, M. 2005, ApJ, 629, 1034
Visvanathan, N. 1967, MNRAS, 135, 275
Voors, R. H. M., et al. 2000, A&A, 356, 501
Walborn, N. R. 1976, ApJ, 204, L17
Walborn, N. R., Blanco, B.M., & Thackeray, A. D. 1978, ApJ, 219, 498
Walsh, J. R., & Ageorges, N. 2000, A&A, 357, 255
Warren-Smith, R. F., Scarrott, S. M., Murdin, P., & Bingham, R. C. 1979, MNRAS, 187, 761
Westphal, J. A., & Neugebauer, G. 1969, ApJ, 156, L45
Whitelock, P. A., et al. 1983, MNRAS, 203, 385
Zethson, T., Gull, T. R., Hartman, H., Johansson, S., Davidson, K., & Ishibashi, K. 2001, AJ, 122, 322